Journal of Hazardous Materials 174 (2010) 398–403

Contents lists available at ScienceDirect

Journal of Hazardous Materials

journal homepage: www.elsevier.com/locate/jhazmat

Adsorptive removal of Congo red, a carcinogenic textile dye, from aqueous solutions by maghemite nanoparticles

Abbas Afkhami*, Razieh Moosavi

Faculty of Chemistry, Bu-Ali Sina University, Hamadan, Iran

ARTICLE INFO

Article history:
Received 16 July 2009
Received in revised form 6 September 2009
Accepted 14 September 2009
Available online 19 September 2009

Keywords:
Congo red adsorption
Maghemite nanoparticles
Waste water samples

ABSTRACT

The adsorption of Congo red (CR) onto maghemite nanoparticles (γ-Fe_2O_3) and its desorption was investigated. The adsorption capacity was evaluated using both the Langmuir and Freundlich adsorption isotherm models. Maghemite nanoparticles (γ-Fe_2O_3) were prepared easily in a surfactant-less microemulsion by co-precipitation method. The size of the produced maghemite nanoparticles was determined by X-ray diffraction (XRD) analysis and scanning electron microscopy (SEM). Synthesized maghemite nanoparticles showed the highest adsorption capacities of CR compared to many other adsorbents and would be a good method to increase adsorption efficiency for the removal of CR in a wastewater treatment process. The maximum adsorption occurred at pH 5.9. The Langmuir adsorption capacity (q_{max}) was found to be 208.33 mg g^{-1} of the adsorbent.

1. Introduction

In the past decade, the synthesis of spinel magnetite and maghemite nanoparticles has been intensively developed not only for its great fundamental scientific interest but also for many technological applications in biology, such as extraction of genomic DNA [1], contrast agents in magnetic resonance imaging (MRI) [2–3], medical applications (such as targeted drug delivery) [4–6], bioseparation [7], and separation and preconcentration of various anions and cations [8–10] due to their structural, electronic, magnetic and catalytic properties. Recently, nano-sized iron oxide particles were widely used in different industrial processes like manufacturing of semiconductors, recording materials, catalysts, gas sensors materials, etc. [6,11]. Because of many novel physical and chemical properties, different methods of synthesis of nanostructure Fe_2O_3 particles were intentionally studied. Numerous chemical methods can be used to synthesize magnetic nanoparticles such as microemulsions [12], sol–gel synthesis [13], sonochemical reactions [14], hydrolysis and thermolysis of precursors [15], flow injection synthesis [16], and electrospray synthesis [17]. The most common method for the production of magnetite nanoparticles is the chemical co-precipitation technique of iron salts [1,18,19]. The co-precipitation technique is probably the simplest and most efficient chemical pathway to obtain magnetic particles. The main advantage of the co-precipitation process is that a large amount of nanoparticles can be synthesized [6].

Color is the first contaminant to be recognized in wastewater. Dyes are used in different industries such as paper and plastics, leather, pharmaceutical, food, cosmetics, dyestuffs, textiles, etc. to color the products. As a result, considerable amount of colored wastewater is generated. The presence of these dyes in water even at very low concentration is highly visible and undesirable [20]. The degradation by-products of organic dyes such as synthetic azo-dyes have dangerous impacts on the environment since it contains toxic aromatic amine compounds and the removal rate of these materials during aerobic waste treatment are still low [11]. Congo red [1-naphthalene sulfonic acid, 3,30-(4,40-biphenylenebis (azo)) bis (4-amino-)disodium salt, CR] is a benzidine-based anionic disazo dye, i.e. a dye with two azo groups. It is toxic to many organisms and is a suspected carcinogen and mutagen. Benzidine, a human carcinogen, and CR are, however, banned in many countries because of health concerns. But, it is still widely used in several countries. Synthetic dyes, such as CR, are difficult to biodegrade due to their complex aromatic structures, which provide them physicochemical, thermal and optical stability [21]. Therefore, there is an urgent requirement for development of innovative, but low-cost processes, by which dye molecules can be removed. Adsorption technique is quite popular due to simplicity and high efficiency, as well as the availability of a wide range of adsorbents [22,23]. Various adsorbents have been tested and used for the removal of dyes from polluted water [24,25]. A number of non-conventional adsorbents such as montmorillonite [26,27], bentonite [28,29], rice hull ash [30], leaf [31], fly ash [32], activated red mud [33], rice husk [34], fungi [35,36], coir pith carbon [37], mesoporous activated carbons [38], anilinepropylsilica xerogel [39], *Azadirachta indica* leaf powder [40], chitosan [41], and mesoporous Fe_2O_3 [42] have been used

* Corresponding author. Tel.: +98 811 8272404 fax: +98 811 8272404.
E-mail address: afkhami@basu.ac.ir (A. Afkhami).

0304-3894/$ – see front matter © 2009 Elsevier B.V. All rights reserved.
doi:10.1016/j.jhazmat.2009.09.066

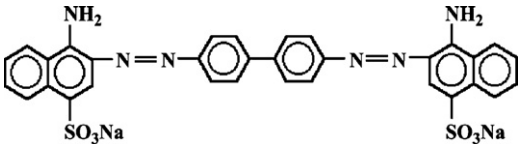

Scheme 1. Molecular structure of CR.

for the removal of CR from aqueous solutions. However, some of these adsorbents do not have good adsorption capacities for anionic dyes.

In the present paper maghemite nanoparticles were employed for removal of CR and used as an effective adsorbent in the wastewater treatment. The technique was found to be very useful and cost-effective for a better removal of dye. These particles showed the highest adsorption capacities of CR compared to many other adsorbents.

2. Experimental

2.1. Instrumentation

A Metrohm model 713 pH-meter was used for pH measurements. A single beam UV-mini-WPA spectrophotometer was used for determination of CR concentration in the solutions. Scanning electron microscope (SEM, VEGA, TESCAN Czech Republic) was used for preparation of SEM images. The crystal structure of synthesized materials was determined by an X-ray diffractometer (XRD) (38066 RIVA, d/G.Via M. Misone, 11/D (TN) ITALY) at ambient temperature. A $40 \pm 5\%$ kHz Parsonic-mini ultrasonic water bath (Pars Nahand, Iran) was used. The BET surface area, pore volume and pore size distribution of the catalyst were measured using N_2 adsorption/desorption technique at 77 K on a Belsorp adsorption/desorption using data analysis software (Bel Japan, Inc.).

2.2. Reagents and materials

All the chemicals and reagents used in this work were of analytical grade and purchased from Merck (Merck, Darmstadt, Germany). A stock solution (1000 mg L^{-1}) of CR (its structure as shown in Scheme 1) was prepared in double distilled water (DDW), and experimental solutions of desired CR concentrations were obtained by successive dilutions of the stock solution with DDW. The concentration of CR in the experimental solution was determined from the calibration curve prepared by measuring absorbance of different predetermined concentrations of CR solutions at 498 nm (λ_{max}).

2.3. Synthesis of maghemite

The maghemite nanoparticles were synthesized according to a co-precipitation method followed by aeration oxidation proposed elsewhere [6,18], except that ultrasonic vibration by an ultrasonic bath was used instead of magnetic stirring. Firstly 3 mL of $FeCl_3$ (2 mol L^{-1} dissolved in 2 mol L^{-1} HCl) was added to 10.33 mL DDW. Then 2 mL of 1 mol L^{-1} Na_2SO_3 solution was added to the former solution dropwise in 1 min ultrasonic vibration for a few minutes leading to smaller and more homogenized particles. Just after mixing the solutions, the color of the solution changed from light yellow to red, indicating complex ions formed between the Fe^{3+} and SO_3^{2-}. After turning the color of solution again, the solution was added to 80 mL of 0.85 mol L^{-1} NH_3 solution under ultrasonic vibration. A black precipitate quickly formed, which was allowed to crystallize completely for another 30 min. The precipitate was washed with DDW by magnetic decantation until the pH of the suspension was less than 7.5. A 170 mL water was added to this suspension and the pH was adjusted to 3.0 with 0.1 mol L^{-1} HCl and was kept stable for 5 min. The suspension was refluxed under aeration (with air) for 60 min at about 100°C until the color of the suspension slowly changed from black to reddish-brown. The solution was washed with DDW by magnetic decantation for several times and the suspension was dried into powder.

2.4. Adsorption behavior of CR

Adsorption studies were performed by adding 0.015 g maghemite nanoparticles to the 50 mL solution of different concentrations of CR in a 250 mL beaker. The pH of the CR solution was adjusted at 5.9 using 0.01 mol L^{-1} HCl and/or 0.1 mol L^{-1} NaOH and the solution was stirred for 30 min. Then CR loaded maghemite nanoparticles were separated with magnetic decantation and centrifugation at 3800 rpm for 3 min. The concentration of CR in the solution was measured spectrophotometrically at 498 nm. The concentration of CR decreased with time due to its adsorption by maghemite.

3. Results and discussion

3.1. Characterization of the adsorbent

The SEM image of the particles, as shown in Fig. 1, revealed the average diameter of maghemite nanoparticles synthesized in this study around 45 nm. As Fig. 1 shows the average diameter of nanoparticles that were prepared using ultrasonic stirring is smaller than those prepared using magnetic stirring. Because ultrasonic irradiation dispersed nanoparticles and therefore prevented their aggregation. The difference of the sizes of nanoparticles was obvious among SEM images.

The typical XRD profile of maghemite nanoparticles is shown in Fig. 2. We calculated the crystallite size measurement around 8.78 nm from the XRD pattern according to Scherrer equation:

$$D = \frac{K\lambda}{(b \cos \theta)} \quad (1)$$

The equation uses the reference peak width at angle θ, where λ is the wavelength of incident X-ray (1.5418 Å), b is the width of the XRD peak at half height and K is a shape factor, about 0.9 for magnetite and maghemite [18,43]. It should be noted that the particle dimension obtained by SEM is higher than the corresponding crystallite size, i.e. 8.78 nm. This difference may be explained due to the presence of aggregates in SEM grain consisting of several crystallites and/or poor crystallinity [44].

The specific surface area of maghemite nanoparticles, obtained by BET analysis, was 81.61 m^2 g^{-1}, and the mean pore diameter was 10.37 nm, with a total pore volume of 0.2116 cm^3 g^{-1}.

3.2. Effect of contact time

The effect of contact time on the adsorption of CR was studied to determine the time taken by maghemite nanoparticles to remove 20.0 and 30.0 mg L^{-1} CR solution at pH 5.9. A 0.05 g of maghemite nanoparticles was added into a 50 mL of CR solution. Absorbance of the solution at 498 nm with time was determined to monitor the CR concentration. The results are shown in Fig. 3. The decrease in the concentration of CR with time is due to its adsorption on maghemite nanoparticles. It can be seen that in about 30 min, almost all the CR became adsorbed. Agitation time of 30 min was selected for further works.

3.3. Effect of pH

The effect of pH in the range 4.0–7.6 on the removal of CR was investigated using 0.01 mol L^{-1} HCl or NaOH solu-

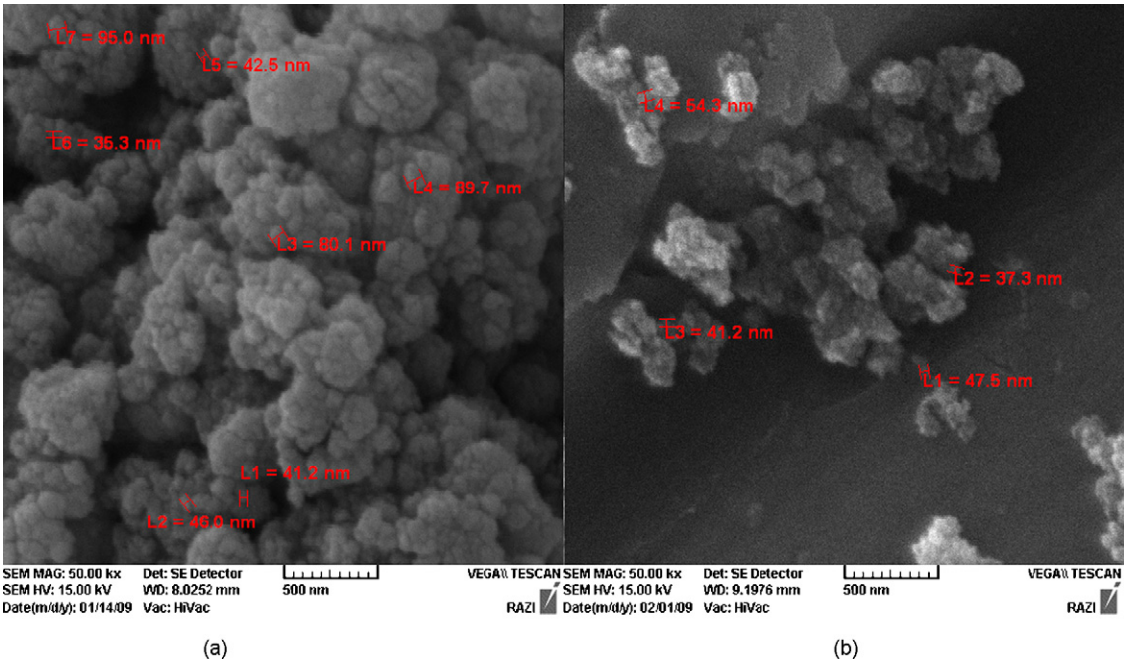

Fig. 1. SEM image of maghemite nanoparticles prepared by magnetic stirring (a) and by use of ultrasonic vibration (b).

tions for pH adjustment, with the initial CR concentration fixed at 2.0×10^{-5} mol L^{-1}. As Fig. 4 shows, the percent adsorption increased by increasing pH and reached maximum at pH 5.9 and then decreased at higher pHs. At higher pHs, the high negatively charged adsorbent surface sites did not favor the adsorption of deprotonated CR due to electrostatic repulsion.

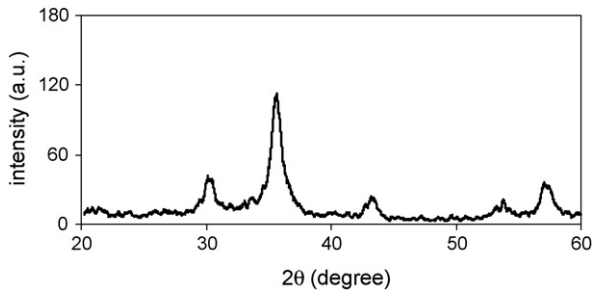

Fig. 2. XRD patterns of the maghemite nanoparticles.

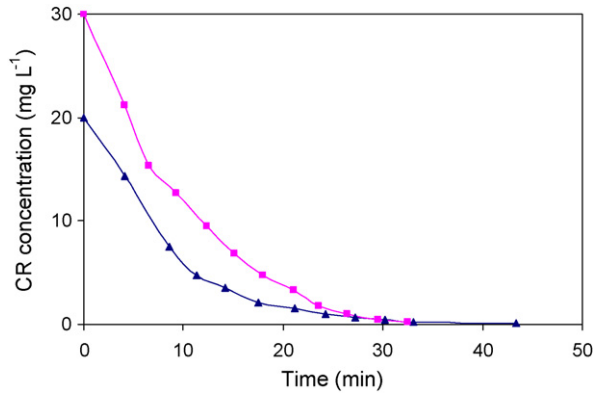

Fig. 3. Adsorption behavior of (▲) 20.0 and (■) 30.0 mg L^{-1} CR on maghemite nanoparticles. Amount of maghemite nanoparticles are 0.0500 g and pH of the solutions is 5.9.

3.4. Mechanism of the adsorption

The surfaces of metal oxides (γ-Fe_2O_3 suspension) are generally covered with hydroxyl groups that vary in forms at different pHs. The surface charge is neutral at pH_{zpc} (the pH of zero point charge, pH_{zpc}, of maghemite nanoparticles is around 6.3 [34]). Below the pH_{zpc}, the adsorbent surface is positively charged, and anion adsorption occurs. As the pH of the CR solution increased, a proportional decrease in adsorption took place due to the successive deprotonation of hydroxyl groups on the adsorbent and electrostatic repulsion between negatively charged sites on the adsorbent and dye anions. There was also competition between OH^- (at high pH) and dye anions for positively charged adsorption sites [21]. Also, CR can become adsorbed onto the metal oxide surface by coordination effect between metal ions and amine groups at the ends of CR molecules [42]. So it is apparent that metal oxides with the higher surface area can adsorb more CR molecules.

3.5. Adsorption isotherms

The equilibrium adsorption isotherm model, which is the number of mg adsorbed per gram of adsorbent (q_e) vs. the equilibrium concentration of adsorbate (Fig. 5), is fundamental in describing the

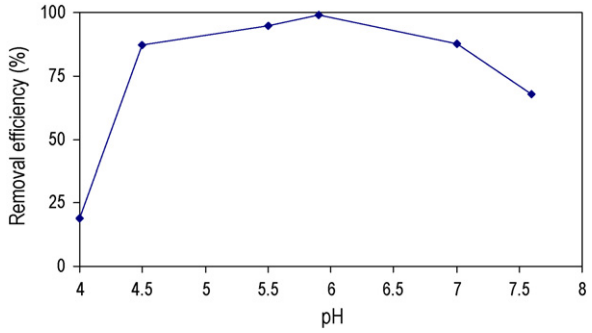

Fig. 4. Removal of CR in various pHs. Conditions: 0.05 g maghemite, 20 mL of 30 mg L^{-1} Mo(VI), agitation time of 30 min.

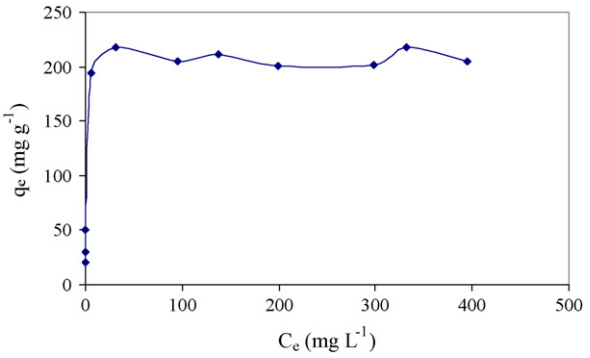

Fig. 5. Plots of q_e vs. C_e for the adsorption of CR onto maghemite nanoparticles. Conditions: pH 5.9, 0.1 g maghemite.

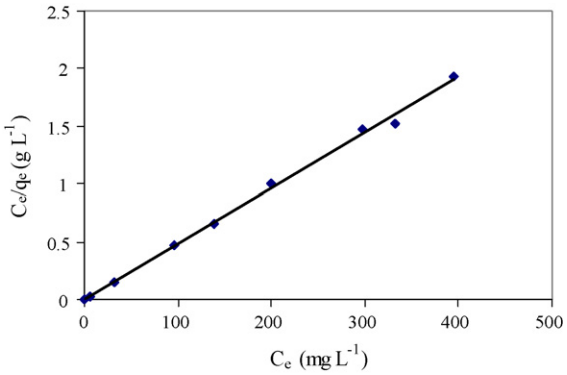

Fig. 6. Linearization of the Langmuir isotherm. Conditions: pH 5.9, 0.1 g maghemite.

interactive behavior between adsorbate and adsorbent. Analysis of isotherm data is important for predicting the adsorption capacity of the adsorbent, which is one of the main parameters required for the design of an adsorption system. Equilibrium isotherm studies were carried out with different initial concentrations of CR (20–600 mg L^{-1}) at 25 °C and pH 5.9. Two models were used to analyze the equilibrium adsorption data: Langmuir [45] and Freunlich [46]. Langmuir's model does not take into account the variation in adsorption energy, but it is the simplest description of the adsorption process. It is based on the physical hypothesis that the maximum adsorption capacity consists of a monolayer adsorption, that there are no interactions between adsorbed molecules, and that the adsorption energy is distributed homogeneously over the entire coverage surface [21,22].

The general form of the Langmuir isotherm is:

$$\frac{q_e\, a_L}{K_L} = \frac{K_L C_e}{(1 + K_L C_e)} \tag{2}$$

where C_e is the equilibrium concentration of the CR in the solution (mg L^{-1}), q_e is the amount of CR adsorbed per unit mass of adsorbent (mg g^{-1}), at equilibrium concentration, C_e, a_L (L mg^{-1}) and K_L (L g^{-1}) are the Langmuir constants with a_L related to the adsorption energy and q_m [=K_L/a_L] signifies the maximum adsorption capacity (mg g^{-1}), which depends on the number of adsorption sites. The Langmuir isotherm shows that the amount of anions adsorbed increases as the concentration increases up to a saturation point. As long as there are available sites, adsorption will increase with increasing CR concentrations, but as soon as all of the sites are occupied, a further increase in concentrations of CR solutions does not increase the amount of CR on adsorbents [21,22].

After linearization of the Langmuir isotherm, Eq. (3), we obtain:

$$\frac{C_e}{q_e} = C_e \left(\frac{a_L}{K_L}\right) + \left(\frac{1}{K_L}\right) \tag{3}$$

The values of a_L and K_L are calculated from the slope and intercept of the plot of *Ce*/*qe* vs. *Ce* (Fig. 6). The amount of CR adsorbed (mg g^{-1}) was calculated based on a mass balance equation as given below:

$$q_e = \frac{V(C_O - C_e)}{m} \tag{4}$$

where C_o is the initial concentration of CR in mg L^{-1}, V is the volume of experimental solution in L, and m is the dry weight of nanoparticles in g. The parameters of the Langmuir equation were calculated and are given in Table 1. Table 1 indicates that the maximum adsorption capacity of maghemite nanoparticles (q_m = 208.33 mg g^{-1}) for CR is very much higher than that of other adsorbents. The essential feature of the Langmuir isotherm can be expressed in terms of a dimensionless constant separation factor (R_L) given by the following equation:

$$R_L = \frac{1}{(1 + a_L C_o)} \tag{5}$$

R_L values within the range $0 < R_L < 1$ indicate favorable adsorption [29]. In this study, R_L value of maghemite nanoparticles for the initial CR concentration of 100 mg L^{-1}, obtained as 0.00146, indicate favorable adsorption of CR onto them.

The Freundlich isotherm model is an empirical equation that describes the surface heterogeneity of the sorbent. It considers multilayer adsorption with a heterogeneous energetic distribution of active sites, accompanied by interactions between adsorbed molecules [21]. The Freundlich empirical model is represented by:

$$q_e = K_f C_e^{1/n} \tag{6}$$

where C_e is the equilibrium concentration (mg L^{-1}), q_e is the amount adsorbed at equilibrium (mg g^{-1}), and K_f (mg$^{1-1/n}$ $L^{1/n}$ g^{-1}) and $1/n$ are Freundlich constants depending on the temperature and the given adsorbent–adsorbate couple. n is related to the adsorption energy distribution, and K_f indicates the adsorption capacity. The linearized form of the Freundlich adsorption isotherm equation is

$$\ln q_e = \ln K_f + \left(\frac{1}{n}\right) \ln C_e \tag{7}$$

The values of K_f and $1/n$ calculated from the intercept and slope of the plot of ln q_e vs. ln C_e are listed in Table 1. Table 1 shows that the values of correlation coefficient, r, for the fit of experimental isotherm data to Langmuir equation is more close to 1.0000 than that for Frendlich equation. Therefore, the Langmuir model represents the experimental data better on the basis of values of regression coefficients.

3.6. Performance evaluation

The maximum adsorption capacity (q_{max}) for the adsorption of CR on γ-Fe_2O_3 nanoparticles calculated from the Langmuir isotherm model is listed in Table 2 with literature values of q_{max} of other adsorbents for CR adsorption [21,27–29,31–33,

Table 1
Parameters of Langmuir and Freundlich isotherm equations, regression coefficients (r) for the adsorption of CR on maghemite nanoparticles at 25 °C and at pH 5.9.

Langmuir	a_L (L mg^{-1})	K_L (L g^{-1})	K_L/a_L[=q_m] (mg g^{-1})	R_L*	r
	6.857	1428.57	208.33	0.00146	0.9991
Freundlich	K_f (mg$^{1-1/n}$ $L^{1/n}$ g^{-1})		$1/n$		r
	35.56		0.3241		0.9442

*For CR concentration of 100 mg L^{-1}.

Table 2
Summary of CR adsorption capacities of various adsorbents.

Type of adsorbent	q_{max}(mg g^{-1})	Reference
CTAB modified chitosan beads	352.5	[21]
Chitosan/montmorillonite nanocomposite	54.52	[27]
Montmorillonite	12.70	[27]
Ca-bentonite	107.41	[28]
Bentonite	158.7	[29]
Neem leaf powder	41.20	[31]
Bagasse fly ash	11.89	[32]
Activated carbon (Laboratory grade)	1.88	[32]
Acid activated red mud	7.08	[33]
$NaHCO_3$ pretreated Aspergillus niger biomass	8.19	[35]
Activated carbon prepared from coir pith	6.70	[37]
Mesoporous activated carbons	189	[38]
Anilinepropylsilica xerogel	22.62	[39]
Chitosan beads	93.71	[41]
Mesoporous Fe_2O_3	53	[42]
N,O-carboxymethyl chitosan	330.62	[47]
4-Vinyl pyridine grafted poly (ethylene terephthalate) fibers	18.1	[48]
Maghemite nanoparticles	208.33	Present work

35,37–39,41,42,47,48]. All of the adsorbents used for CR adsorption have considerably lower q_{max} values than γ-Fe_2O_3 used in this study, except N,O-carboxymethyl chitosan [47] and CTAB modified chitosan beads [21]. However, the simplicity of the preparation method and upon magnetic and electronic properties that cause simple magnetic separation of γ-Fe_2O_3 nanoparticles makes these particles better adsorbent than the others for CR adsorption.

3.7. Regeneration studies

Desorption studies help to elucidate the nature of adsorption and recycling of the spent adsorbent and the CR. pH of the experimental solution influenced CR adsorption inversely. Desorption process was performed on loaded nanoparticles by mixing 0.01 g CR loaded maghemite nanoparticle with 5 mL of EtOH, DMF and 0.01 mol L^{-1} NaOH, solutions and the desorption efficiency for them was calculated as 4, 13, and 95%, respectively. Therefore, the dye could be desorbed from the loaded nanoparticles by changing the pH of the solution to alkaline range and NaOH solution has higher desorption efficiency compared to the other eluents.

4. Conclusion

In summary, γ-Fe_2O_3 nanoparticles with well defined diameter (45 nm) were prepared by such a simple, time-saving and low-cost procedure, in a surfactant-less microemulsion, using partial reduction co-precipitation method combined with ultrasonic stirring. These nanoparticles have relatively high adsorption as compared to the similar materials. The size of the produced maghemite nanoparticles was determined by X-ray diffraction (XRD) analysis and scanning electron microscopy (SEM). UV–vis absorption spectroscopy was used to record the adsorption behavior of the solution after treatment. The characteristic light absorption of CR at 498 nm was chosen to monitor the process of adsorption. The adsorption isotherm data for the CR was derived at room temperature and treated according to Langmuir and Freundlich models. Langmuir model is almost more successful in representing experimental isotherm data for the adsorption of CR on maghemite nanoparticles than the Freundlich model.

Acknowledgements

The authors acknowledge to Bu-Ali Sina University Research Council and Center of Excellence in Development of Chemical Methods (CEDCM) for support of this work.

References

[1] X. Xie, X. Zhang, B. Yu, H. Gao, H. Zhang, W. Fei, Rapidextraction of genomic DNA from saliva for HLA typing on microarray based on magnetic nanobeads, J. Magn. Magn. Mater. 280 (2004) 164–168.
[2] J.W.M. Bulte, Intracellular endosomal magnetic labeling of cells, Methods Mol. Med. 124 (2006) 419–439.
[3] M. Modo, M. Hoehn, J.W.M. Bulte, Cellular MR imaging, Imaging 4 (2005) 143–164.
[4] I. Koh, X. Wang, B. Varughese, L. Isaacs, S.H. Ehrman, D.S. English, Magnetic iron oxide nanoparticles for biorecognition: evaluation of surface coverage andactivity, J. Phys. Chem. B 110 (2006) 1553–1558.
[5] C. Sun, J.S.H. Lee, M. Zhang Zhang, Magnetic nanoparticles in MR imaging and drug delivery, Adv. Drug Deliver. Rev. 60 (2008) 1252–1265.
[6] S. Laurent, D. Forge, M. Port, A. Roch, C. Robic, L. Vander Elst, R.N. Muller, Magnetic iron oxide nanoparticles: synthesis, stabilization, vectorization physicochemical characterizations, and biological applications, Chem. Rev. 108 (2008) 2064–2110.
[7] S. Bucak, D.A. Jones, P.E. Laibinis, T.A. Hatton, Protein separations using colloidal magnetic nanoparticles, Biotechnol. Prog. 19 (2003) 477–484.
[8] B.R. White, B.T. Stackhouse, J.A. Holcombe, Magnetic γ-Fe2O3 nanoparticles coated with poly-L-cysteine for chelation of As(III), Cu(II), Cd(II), Ni(II), Pb(II) and Zn(II), J. Hazard. Mater. 161 (2009) 848–850.
[9] L. Zhou, Y. Wang, Z. Liu, Q. Huang, Characteristics of equilibrium, kinetics studies for adsorption of Hg(II), Cu(II), and Ni(II) ions by thioureamodified magnetic chitosan microspheres, J. Hazard. Mater. 161 (2009) 995–1002.
[10] T. Tuutijärvi, J. Lu, M. Sillanp, G. Chen, As(V) adsorption on maghemite nanoparticles, J. Hazard. Mater. 166 (2009) 1415–1420.
[11] M.H. Khedr, K.S.A. Halim, N.K. Soliman, Synthesis and photocatalytic activity of nano-sized iron oxides, Mater. Lett. 63 (2009) 598–601.
[12] A.B. Chin, I.I. Yaacob, Synthesis and characterization of magnetic iron oxide nanoparticles via w/o microemulsion and Massart's procedure, J. Mater. Process. Technol. 191 (2007) 235–237.
[13] C. Albornoz, S.E. Jacobo, Preparation of a biocompatible magnetic film from an aqueous ferrofluid, J. Magn. Magn. Mater. 305 (2006) 12–15.
[14] E.H. Kim, H.S. Lee, B.K. Kwak, B.K. Kim, Synthesis of ferrofluid with magnetic nanoparticles by sonochemical method for MRI contrast agent, J. Magn. Magn. Mater. 289 (2005) 328–330.
[15] M. Kimata, D. Nakagawa, M. Hasegawa, Preparation of monodisperse magnetic particles by hydrolysis of iron alkoxide, Powder Technol. 132 (2003) 112–118.
[16] G.S. Alvarez, M. Muhammed, A.A. Zagorodni, Novel flow injection synthesis of iron oxide nanoparticles with narrow size distribution, Chem. Eng. Sci. 61 (2006) 4625–4633.
[17] S. Basak, D.-R. Chen, P. Biswas, Electrospray of ionic precursor solutions to synthesize iron oxide nanoparticles: Modified scaling law; Chem, Eng. Sci. 62 (2007) 1263–1268.
[18] Y.K. Sun, M. Ma, Y. Zhang, N. Gu, Synthesis of nanometer-size maghemite particles from magnetite, Colloids Surf. A 245 (2004) 15–19.
[19] A. Kumar Gupta, M. Gupta, Synthesis and surface engineering of iron oxide nanoparticles for biomedical applications, Biomaterials 26 (2005) 3995–4021.
[20] R. Jain, S. Sikarwar, Photocatalytic and adsorption studies on the removal of dye Congo red from wastewater, Int. J. Environ. Pollut. 27 (2006) 158–178.
[21] S. Chatterjee, D.S. Lee, M.W. Lee, S.H. Wooa, Enhanced adsorption of congo red from aqueous solutions by chitosan hydrogel beads impregnated with cetyl trimethyl ammonium bromide, Bioresour. Technol. 100 (2009) 2803–2809.
[22] A. Afkhami, T. Madrakian, A. Amini, Mo(VI) and W(VI) removal from water samples by acid-treated high area carbon cloth, Desalination 243 (2009) 258–264.
[23] A. Afkhami, T. Madrakian, A. Amini, Z. Karimi, Effect of the impregnation of carbon cloth with ethylenediaminetetraacetic acid on its adsorption capacity for the adsorption of several metal ions, J. Hazard. Mater. 150 (2008) 408–412.
[24] G. Crini, Non-conventional low-cost adsorbents for dye removal: A review, Bioresour. Technol. 97 (2006) 1061–1085.
[25] S.J. Allen, G. McKay, J.F. Porter, Adsorption isotherm models for basic dye adsorption by peat in single and binary component systems, J. Colloid Interface Sci. 280 (2004) 322–333.
[26] Z. Yermiyahu, I. Lapides, S. Yariv, Visible absorption spectroscopy study of the adsorption of Congo Red by montmorillonite, Clay Miner. 38 (2003) 483–500.
[27] L. Wang, A. Wang, Adsorption characteristics of congo red onto the chitosan/montmorillonite nanocomposite, J. Hazard. Mater. 147 (2007) 979–985.
[28] L. Lian, L. Guo, C. Guo, Adsorption of congo red from aqueous solutions onto Ca-bentonite, J. Hazard. Mater. 161 (2009) 126–131.
[29] E. Bulut, M. Ozacar, I.A. Sengil, Equilibrium and kinetic data and process design for adsorption of Congo Red onto bentonite, J. Hazard. Mater. 154 (2008) 613–622.
[30] K.S. Chou, J.C. Tsai, C.T. Lo, The adsorption of congo red and vacuum pump oil by rice hull ash, Bioresour. Technol. 78 (2001) 217–219.
[31] K.G. Bhattacharrya, A. Sharma, *Azadirachta indica* leaf powder as an effective biosorbent for dyes: a case study with aqueous congo red solutions, J. Environ. Manage. 71 (2004) 217–229.
[32] I.D. Mall, V.C. Srivastava, N.K. Agarwal, I.M. Mishra, Removal of congo red from aqueous solution by bagasse fly ash and activated carbon: kinetic study and equilibrium isotherm analyses, Chemosphere 61 (2005) 492–501.
[33] A. Tor, Y. Cengeloglu, Removal of congo red from aqueous solution by adsorption onto acid activated red mud, J. Hazard. Mater. 138 (2006) 409–415.

[34] R. Han, D. Ding, Y. Xu, W. Zou, Y. Wang, Y. Li, L. Zou, Use of rice husk for adsorption of congo red from aqueous solution in column mode, Bioresour. Technol. 99 (2008) 2938–2946.
[35] Y. Fu, T. Viraraghavan, Removal of congo red from an aqueous solution by fungus Aspergillus niger, Adv. Environ. Res. 7 (2002) 239–247.
[36] A.R. Binupriya, M. Sathishkumar, K. Swaminathan, C.S. Ku, S.E. Yun, Comparative studies on removal of congo red by native and modified mycelial pellets of Trametes versicolor in various reactor modes, Bioresour. Technol. 99 (2008) 1080–1088.
[37] C. Namasivayam, D. Kavitha, Removal of congo red from water by adsorption onto activated carbon prepared from coir pith, an agricultural solid waste, Dyes Pigments 54 (2002) 47–58.
[38] E.L. Grabowska, G. Gryglewicz, Adsorption characteristics of congo red on coal-based mesoporous activated carbon, Dyes Pigments 74 (2007) 34–40.
[39] F.A. Pavan, S.L.P. Dias, E.C. Lima, E.V. Benvenutti, Removal of congo red from aqueous solution by anilinepropylsilica xerogel, Dyes Pigments 76 (2008) 64–69.
[40] K.G. Bhattacharyya, A. Sharma, *Azadirachta indica* leaf powder as an effective biosorbent for dyes: a case study with aqueous congo red solutions, J. Environ. Manage. 71 (2004) 217–229.
[41] S. Chatterjee, S. Chatterjee, B.P. Chatterjee, A.K. Guha, Adsorptive removal of congo red, a carcinogenic textile dye by chitosan hydrobeads: binding mechanism, equilibrium and kinetics, Colloids Surf. A 299 (2007) 146–152.
[42] C. Yu, X. Dong, L. Guo, J. Li, F. Qin, L. Zhang, J. Shi, D. Yan, Template-Free Preparation of Mesoporous Fe2O3 and Its Application as Absorbents, J. Phys. Chem. C 112 (2008) 13378–13382.
[43] J. Hu, G. Chen, I.M.C. Lo, Removal and recovery of Cr(VI) from wastewater by maghemite nanoparticles, Water. Res. 39 (2005) 4528–4536.
[44] R.N. Panda, M.F. Hsieh, R.J. Chung, T.S. Chin, FTIR, XRD, SEM and solid state NMR investigations of carbonate-containing hydroxyapatite nano-particles synthesized by hydroxide-gel technique, J. Phys. Chem. Solids 64 (2003) 193–199.
[45] L. Langmuir, The adsorption of gases on plane surfaces of glass, mica and platinum, J. Am. Chem. Soc. 40 (1918) 1361–1403.
[46] H. Freundlich, W. Heller, The Adsorption of cis- and trans-Azobenzene, J. Am. Chem. Soc. 61 (1939) 2228–2230.
[47] L. Wang, A. Wang, Adsorption properties of congo red from aqueous solution onto N, O-carboxymethly-chitosan, Bioresour. Technol. 99 (2008) 1403–1408.
[48] M. Arslan, M. Yiğitoğlu, Adsorption behavior of congo red from an aqueous solution on 4-vinyl pyridine grafted poly (ethylene terephthalate) fibers, J. Appl. Polym. Sci. 107 (2008) 2846–2853.